15th AIAA/CEAS Aeroacoustics Conference (30th AIAA Aeroacoustics Conference)
11 - 13 May 2009, Miami, Florida

AIAA 2009-3326

Experiments on Shielding of Jet Noise by Airframe Surfaces

Dimitri Papamoschou* and Salvador Mayoral†
University of California, Irvine, CA 92697, USA

We present parametric subscale experimental studies of jet noise shielding in two basic configurations. The first configuration used a single-stream Mach 0.9 cold air jet with a rectangular shield. The second configuration was composed of a dual-stream bypass ratio 10 nozzle that operated at realistic cycle conditions and a hybrid-wing body (HWB) planform shield. For both configurations, the shield was adjustable relative to the nozzle. Tabs, chevrons, and wedge fan flow deflectors were added to the nozzles to compact the noise source region. Aeroacoustic surveys were conducted inside an anechoic chamber using an eight-microphone polar array. The experiments with the single-stream jet and rectangular shield showed an excess of noise at low frequencies, yet reduced noise at high frequencies. Since the excess noise occurs at low frequencies, it has a minor impact on the perceived noise level of a full-scale engine. Significant EPNL reductions, up to 7.4 dB cumulative (downward plus sideline), were measured with an aft shield length of 5 jet diameters. The addition of mixer tabs increased this benefit to 10.7 dB, even though the jet itself became noisier. The HWB shielding effectiveness with the plain nozzle is marginal, even with the engine translated two fan diameters upstream of its nominal location. However, applying fan flow deflectors or chevrons yielded a significant EPNL benefit, about 6.5 dB cumulative, with the engine positioned at its nominal location. Thus, the compaction and/or redistribution of the noise source are essential for effective jet noise shielding on the HWB. A proposed correlator for the noise reduction due to shielding is the average illumination angle. The experimental data show a trend of increasing EPNL reduction with decreasing average illumination angle. For average illumination angles less than 45 deg, the EPNL reduction in a particular azimuthal direction exceeds 3 dB.

Nomenclature

D_j	=	Jet exit diameter
D_f	=	Fan nozzle exit diameter
f	=	Frequency
M	=	Mach number
Sr	=	Strouhal number
U	=	Velocity
x,y,z	=	Axial, transverse, and spanwise coordinates relative to nozzle exit
X_n	=	Noise source length
X_s, Y_s, Z_s	=	Shield trailing edge location relative to nozzle exit
θ	=	Polar angle from jet axis
ϕ	=	Azimuth angle
ψ	=	Illumination angle
$\bar{\psi}$	=	Average illumination angle
BPR	=	Bypass ratio
EPNL	=	Effective perceived noise level
HWB	=	Hybrid wing body
NPR	=	Nozzle pressure ratio
TE	=	Trailing edge
OASPL	=	Overall sound pressure level
PNL	=	Perceived noise level

* Professor, Department of Mechanical and Aerospace Engineering, dpapamos@uci.edu, AIAA Fellow.
† Graduate Student Researcher, Department of Mechanical and Aerospace Engineering, smayoral@uci.edu AIAA Student Member.

I. Introduction

THIS study is motivated by the development of ultra-quiet advanced aircraft that shield jet noise with airframe surfaces. In such aircraft the engines would be mounted over-the-wing (OTW) to utilize the wing as a sound barrier between the emitted exhaust noise and the ground observer. Significant experimental research on the OTW concept for conventional and short-takeoff airplanes occurred in the 1970s[1-3]. Important trends were established for the changes in the spectrum of acoustic emission versus shield parameters. However, the investigations were not extensive enough to develop high-fidelity empirical tools for jet noise shielding prediction. In addition, there was little emphasis on the physics of the jet noise source and its interaction with the shield surface. Since then, no significant progress occurred in this research area. Commercially the OTW concept did not find support, with application to only one relatively obscure aircraft, the Fokker VFW614.

The advent of the ultra-efficient hybrid-wing body (HWB) airplane has reinvigorated the OTW concept for jet noise shielding with its top-wing mounted engines. The HWB design provides sufficient planform area to shield both the forward-emitting turbomachinery noise sources and the aft-emitting jet noise sources. To properly integrate the engine with the airframe for jet noise shielding, physics-based predictive tools must be developed. The challenge is that jet noise is a distributed and directive source, whose exact nature remains under investigation. The current "state of the art" in empirical prediction of jet noise shielding approximates the noise source as a small number of discrete sources[4] combined with insertion loss formulas developed for barrier insertion losses of sound from point sources. The insertion loss formula is based on Maekawa's experiments[5] and involves only the Fresnel number. The current state of the art is thus inadequate because jet noise is a distributed source of finite spatial coherence and the barrier-insertion relations were developed for point sources[6].

The absence of reliable physics-based tools for predicting jet noise shielding necessitates the reliance on experimental data. Past papers on OTW experiments provided some useful data but their range was too limited for aircraft noise assessment. It was deemed necessary to conduct a number of parametric studies in a subscale aeroacoustic facility to gain a preliminary assessment of the impact of jet noise shielding on the effective perceived noise level (EPNL), understand the basic nature of the jet noise source (using phased arrays) as it relates to shielding, and generate correlations that will assist in the development of more advanced models of the jet noise source.

II. Experimental Setup

A. Nozzles

Two nozzles were utilized in the subscale experiments. Their pictures and coordinates are shown in Figs. 1 and 2. The first nozzle (Fig.1) was a simple single-stream convergent nozzle with an exit diameter D_j =2.26 cm. The second nozzle (Fig.2) was a dual-stream turbofan-type nozzle with a fan diameter D_f=3.12 cm that yielded a bypass ratio BPR=10 at takeoff cycle conditions. Its design was based on NASA Glenn Research Center's (GRC) 5BB turbofan nozzle, nominally with BPR=8. The bypass ratio was increased to 10 by slightly enlarging the nozzle plug. Both nozzles were manufactured from epoxy resin using stereolithography methods. The single-stream nozzle operated with only cold air at nozzle pressure ratio NPR= 1.7 to produce an exit Mach number of 0.9. The BPR10 nozzle operated with helium-air mixtures in both the core and fan nozzles at the engine cycle conditions listed in Table 1.

B. Mixing Enhancers and Fan Flow Deflectors

Mixing enhancers and fan flow deflectors were utilized to compact and redistribute the noise sources. To enhance mixing between the jet core and ambient air for the single-stream nozzle, four triangular tabs were attached to the lip of the nozzle exit, as shown in Fig. 3. For the BPR10 nozzle, wedge-type fan flow deflectors and chevrons were used. Porous wedge-type fan flow deflectors, fabricated from a fine interwoven metal mesh with a porosity of 49%, were added to the BPR10 nozzle, as illustrated in Fig. 4a. Previous studies on wedge-type fan flow deflectors[7] have shown that porous flaps mitigate the steep velocity gradients that can cause excess noise at high polar angles. The main function of wedge-type deflectors is to reshape the jet flow by thickening the fan flow on the underside of the jet. In addition, there is a significant reduction in the length of the primary potential core. A rather aggressive wedge half angle of 18° was used in the experiments. Such an aggressive design is expected to significantly reduce peak noise in the downward direction but could increase noise emitted in the 90° polar direction for all azimuth angles, especially in the upward direction. Chevrons with a 20° insertion, designed by Boeing, were added to both the core and fan nozzles of the BPR10 nozzle, as shown in Fig. 4b. Chevrons are triangular shaped serrations mounted along the perimeter of the nozzle exit that are slightly immersed into the exhaust stream. They generate a pressure difference between the flows on both sides of the serration that lead to the formation of pairs of stream wise vortices from both side edges of the chevron serration.

C. Shielding Surfaces

The single-stream nozzle was subjected to fundamental parametric shielding studies using a rectangular shield with a 61 cm span and variable chord length. The centerline of the jet was positioned at 1.2 and 1.8 jet diameters above the shield surface, as shown in Fig. 5a. Figure 5b outlines the nozzle-shield configurations and chord lengths used in the study. In the case for the BPR10 nozzle, jet noise shielding came in the form of the HWB airplane airframe. A scaled-down model (by factor of 90) of the HWB planform shape was designed with all of its essential dimensions, as illustrated in Fig. 6. The HWB shield was manufactured from 3.2-mm thick aluminum sheet and features removable/adjustable verticals and a removable/adjustable elevator flap to simulate takeoff and landing. The HWB shield was mounted on a longitudinal traverse that permitted the axial displacement of the nozzle either upstream or downstream from its nominal position. The detailed design of the shield and its integration with the BPR10 nozzle is depicted in Fig. 7.

D. Aeroacoustic Testing

Acoustic tests were conducted inside an anechoic chamber at the University of California, Irvine's Jet Aeroacoustics Facility, depicted in Fig. 8. This subscale facility utilizes a dual-stream apparatus capable of delivering helium-air mixtures to the primary (core) and secondary bypass (fan) nozzles, as shown in Figure 8b. Previous studies have demonstrated that matching exit velocity and Mach number conditions with helium-air mixtures is an effective and inexpensive method to accurately simulate the acoustic behavior of a full-scale heated jet[8]. The single-stream nozzle operated with only cold air at NPR=1.7 to produce an exit Mach number of 0.9. The BPR10 nozzle operated with helium-air mixtures in both the core and fan nozzles at the engine cycle conditions listed in Table 1.

Noise measurements were performed inside an anechoic chamber using a microphone polar array consisting of eight 3.2-mm condenser microphones (Bruel & Kjaer, Model 4138) with a frequency response of 140 kHz. The microphones were mounted on a circular pivot arc centered within the vicinity of the nozzle exit. The polar aperture of the array is 30° and the array radius is 1 m. The angular spacing of the microphones is logarithmic. The entire array structure is rotated around its center in order to position the array at the desired polar angle. Positioning of the array is done remotely using a stepper motor. An electronic inclinometer displays the position of first microphone. The polar angle θ ranged from 20° to 120°. Variations of the azimuth angle were done by rotating the nozzle and shielding surface. This study encompassed the azimuth angles ϕ of 0°, 30°, 60°, 90°, and 120°. The arrangement of the microphones inside the anechoic chamber, and the principal electronic components, are shown in Fig. 8a. The microphones were connected, in groups of four, to two amplifier/signal conditioners (Bruel & Kjaer, Model 4138) with high-pass filter set at 300 Hz and low-pass filter set at 100 kHz. The four-channel output of each amplifier was sampled at 250 kHz per channel by a multi-function data acquisition board (National Instruments PCI-6070E). Two such boards, one for each amplifier, were installed in a Pentium 4 personal computer. National Instruments LabView software was used to acquire the signals. The sound pressure level spectrum for each experimental run was corrected for actuator response, free-field correction, and atmospheric absorption. Integration of the corrected spectrum produced the overall sound pressure level (OASPL). Both sound spectra and OASPL were referenced to a distance of 1.25 D_f from the nozzle exit.

In evaluating the acoustic merits of each configuration Perceived Noise Level (PNL) and Effective Perceived Noise Level (EPNL) were calculated from sound measurements. The calculations are based on a flyover at an altitude of 1500 ft, engine angle of attack of 15°, and an engine thrust level of 70,000 lb. The basic steps of the EPNL estimation procedure are as follows:

- The aircraft position is computed every 0.5-sec interval. For each observation time t, the distance and polar emission angle θ are computed for the "retarded" position
- For each t, the lossless, scaled-up spectrum corresponding to $\theta(t)$ is obtained from the experimental measurements. This requires interpolation between the measured spectra and, for polar angles outside the range covered in the experiment, moderate extrapolation. To enhance the accuracy of interpolation or extrapolation the spectra were smoothed using a Savitzky-Golay filter which removes extraneous fluctuations but preserves the basic shape of the spectrum.
- The spectrum is Doppler-shifted to account for the motion of the aircraft.
- The spectrum is corrected for distance and atmospheric absorption. The absorption correction is applied for ambient temperature 29°C and relative humidity 70%.
- The spectrum is discretized into 1/3-octave bands and the perceived noise level (PNL) is computed according to Part 36 of the Federal Aviation Regulations.

- The above steps result in the time history of perceived noise level, PNL(t). From it, the maximum level of PNL, PNLM, is determined. The duration of PNL exceeding PNLM-10 dB is calculated and the corresponding "duration correction" is computed according to FAR 36[9]. The effective perceived noise level, EPNL, equals PNLM plus the duration correction.

The change in EPNL (ΔEPNL) in the downward ($\phi = 0$ deg) and sideline ($\phi = 60$ deg) directions were used as a preliminary "figure of merit" in the assessment shielding for each configuration. This estimate does not include factors such as aerodynamic effects of forward flight, installation effects, and noise from sources other than turbulent mixing noise (e.g., fan tones, airframe sound) that affect the overall EPNL of a real airplane. However EPNL does include metrics of community noise, duration of noise, and human annoyance.

Noise source mapping is based on the basic DAMAS approach of Brooks and Humphreys[10] with additional features for self-consistent imaging of directional sources as described in Papamoschou[11]. The source images were deconvolved using the Richardson-Lucy inversion method.

III. Aeroacoustic Results

A. Noise Source Maps of the Free Jets

Knowledge of the jet noise source region is essential for the application and prediction of jet noise shielding. Modifications of the jet nozzle, such as mixers and deflectors, can significantly alter the noise source distribution in ways that benefit shielding. Noise source maps for the single-stream Mach 0.9 jet, without and with mixer tabs, are shown in Fig. 9. The noise source maps plot the sound intensity versus axial position, normalized by jet diameter and versus Strouhal number Sr. It is evident that the tabs contract the noise source region as well as shift the peek intensity to a higher frequency. Fig. 10 plots the noise source maps for the unmodified and modified BPR10 jets: baseline, with porous wedge deflectors, and with chevrons. The deflectors reduced sound intensity levels (in the direction shown) and, like the tabs, compacted the noise source region. The chevrons reduced low-frequency noise levels but increased high-frequency noise levels near the nozzle exit.

Plots of the peak noise source location, depicted in Fig. 11, show clearly the compaction of the noise source regions for the single-stream and BPR10 jets affected by the tabs, wedge, and chevrons. The average axial location of the peak noise within the 100-400 Hz band (full-scale, based on 70,000-lb static thrust) is taken here as a measure of the length of the noise source region X_n. Using this definition, for the single-stream jet, the mixer tabs reduced the noise source length to $2.1D_j$ from $3.8D_j$. For the BPR10 jet the baseline case generated a noise source length of $4.57\ D_f$. The addition of the porous wedge and chevrons reduced the noise source length to $1.75\ D_f$ and $2.15\ D_f$, respectively.

B. Key Results of Single-Stream Jet Shielding by Rectangular Plate

Figure 12 presents an acoustic summary of shielding for the Simple jet. Plotted are narrowband spectra at different polar angles θ from the jet axis, OASPL versus θ and PNL versus time and observer polar angle. The figure also includes the estimated reductions in EPNL. At low frequencies, the shield produces excess noise which amplifies with increasing polar angle. Although past works have attributed this excess to scrubbing noise, it may also be a consequence of the directional nature of the jet noise sources. Fortunately, the excess noise occurs at frequencies too low to significantly impact the EPNL for the thrust level considered here (70,000 lb). For higher frequencies, the shield reduces the sound pressure levels. For the particular configuration shown in Fig. 12, there are significant EPNL benefits of 4.4 dB in the downward direction and 3.0 dB in the sideline direction.

The introduction of mixing tabs (and attendant reduction in the noise source region as shown in Fig. 11), increases the noise benefit even more, as demonstrated in Fig. 13. The EPNL benefit in the downward direction rises to 6.2 dB. It should be noted that the free jet with mixer tabs is about 3 dB louder than the plain free jet, so the EPNL reduction relative to the mixer jet is about 9.2 dB.

Significant effort was placed into comparing the UCI data with larger-scale jet noise shielding experiments conducted in the past. Figure 14 presents such a comparison with a NASA experiment[13] that was similar, though not identical to one of the configurations tested at UCI. Figure 14 compares shielded and unshielded spectra. The UCI results were scale-up to the size of the NASA experiment. There is a good match between the spectra for both the shielded and unshielded cased. Cross-over occurs at about 1.2 kHz, similar to the large-scale experiment. This cross-over frequency corresponds to 70 Hz full-scale based on 70,000 lb thrust.

Figure 15 plots the EPNL reduction due to shielding versus aft shield length normalized by the noise source length, X_s/X_n, for two nozzle heights. In these experiments, the nozzle height did not have a major impact on the effectiveness of the shield. It is notable that the shielding with tabs falls along a linear extension of the shielding data with plain nozzle.

C. Key Results of BPR10 Jet Shielded by HWB Planform

A parametric investigation of the BPR10 jet shielding by the HWB planform entailed axial movement of the nozzle about its nominal position and addition of nozzle modifications (wedge and chevrons). Figures 16, 17, and 18 show acoustic results for HWB jet noise shielding using the plain nozzle, perforated-flap fan flow deflectors, and chevrons, respectively. The nozzle is positioned at its nominal location. With the plain nozzle, noise reduction is modest at around 1.0 EPNdB in the downward and sideline directions. The perforated flaps gave an EPNL benefit of 4.3 dB in the downward direction and a 2.3 dB in the sideline direction. The chevrons increased this benefit to around 3.2 EPNdB. Moving the plain nozzle up to two fan diameters upstream of its nominal position yielded marginal benefits, increasing the EPNL reduction to only 1.5 EPNdB. Table 2 summarizes the HWB planform shielding results. The verticals had a significant impact on attenuation of sideline noise. Angles of verticals and elevator had minor effects on the acoustics.

Considering that the noise source region of the plain nozzle extends to 5-6 fan diameters (Fig. 11), it is not surprising that the HWB shield is inadequate to significantly reduce jet noise from the plain nozzle. These results underscore the importance of noise source compaction/redistribution for jet noise shielding.

IV. Correlations

The problem of jet noise shielding is extremely complex and thus not amenable to simple analytical solutions. Accurate predictions require computational models for the noise source and its diffraction from the airframe surface. The resulting computations are expensive and time-consuming, particularly for high frequency. On the other hand, it would be useful to have a preliminary estimate of shielding without having to resort to lengthy computations. Such estimate would help in the preliminary design of shielding configurations. Here we construct a simple model based on the illumination angle, namely the angular sector between source and observer not intercepted by the shield. This is depicted as the angle ψ in Fig. 19. Given that the jet noise source is distributed, we define the average illumination angle $\overline{\psi}$ as follows:

$$\overline{\psi} = \frac{1}{X_n}\int_0^{X_n} \psi dx \tag{1}$$

where the noise source length is based on the peak noise source locations of Fig.11. For a given azimuth angle $\phi = \phi_0$, the illumination angle for source position x depends on the location of the shield trailing edge, relative the position of the source, as determined by the intersection of the trailing edge by the plane $\phi = \phi_0$ passing through the jet axis. This is illustrated in Fig. 19. Denoting the intersection point (X_s, Y_s, Z_s), the average illumination angle is

$$\overline{\psi}(\phi) = \frac{1}{X_n}\int_0^{X_n} \tan^{-1}\left(\frac{\sqrt{Y_s^2(\phi) + Z_s^2(\phi)}}{X_s(\phi) - x}\right) dx \tag{2}$$

This general formulation may include not only the planform trailing edge but also the trailing edge of the verticals. Clearly the formula assumes a large upstream extent of the shield, which may break down in reality, particularly for the verticals. Equation 2 was applied to all the configurations studied with the rectangular and HWB shields. In the latter, the vertical fins were included in the calculation. The calculation was carried out in the downward (ϕ=0°) and sideline (ϕ=60°) planes. The resulting average illumination angle was used as a correlator for the reduction in EPNL due to shielding. This means that, for each nozzle configuration (plain, wedge, chevrons, etc), we calculated the EPNL reduction due to insertion of the shield (this is different from the EPNL reductions cited earlier) and plotted it versus $\overline{\psi}$. This is shown in Fig. 20. The plot includes all the nozzles, all the shields, and all the positions of the nozzles relative to their respective shields. Although there is considerable scatter in the plot, a definite trend is shown of increasing EPNL reduction with decreasing illumination angle. As a rule of thumb, a reduction of 3 EPNdB may be expected if the average illumination angle is 45 deg., and a reduction of as much as 6 EPNdB may be possible by reducing the average illumination angle to about 20 deg. It is important to keep in mind that the EPNL was based on a thrust of 70,000 lb. The trends for much smaller or much larger engines may be different.

V. Conclusion

We conducted parametric subscale experimental studies of jet noise shielding in two basic configurations. The first configuration used a single-stream Mach 0.9 cold air jet with a rectangular shield. The second configuration was composed of a dual-stream BPR10 nozzle that operated at realistic cycle conditions and a HWB planform shield. For both configurations, the shield was moveable relative to the nozzle. Mixing tabs, chevrons, and wedge fan flow deflectors were incorporated into the nozzles to compact the noise source region. Aeroacoustic surveys were conducted inside an anechoic chamber using an eight-microphone polar array.

The experiments with single-stream jet and rectangular shield showed excess noise at low frequencies and reduced noise at high frequencies. The cross-over occurs at Strouhal numbers between 0.5 and 1.0. The excess and reduction amplify with increasing aft shield length. Since the excess noise occurs at low frequencies, it has a minor impact on the perceived noise level of a full-scale engine. The excess noise is believed to be related to the shallow directivity of the Mach 0.9 jet. Significant EPNL reductions, up to 7.4 dB cumulative (downward plus sideline), were measured with an aft shield length of 5 jet diameters. The addition of mixer tabs increased this benefit to 10.7 dB, even though the jet itself became noisier. Noise source location measurements indicate that the mixers reduced the noise source length by about 50%, which explains the increased effectiveness of the shielding.

In the case of the BPR10 nozzle with the HWB shield, the large fan diameter inherent to the high bypass ratio creates a long noise source region. Shielding effectiveness with the plain nozzle is marginal, even with the engine translated two fan diameters upstream of its nominal location. On the other hand, applying the wedge fan flow deflector or the chevrons yielded a significant EPNL benefit, about 6.5 dB cumulative, with the engine positioned at its nominal location. Both devices are shown to compact the noise source region. It became clear that the compaction and/or redistribution of the noise source are essential for effective jet noise shielding on the HWB.

A proposed correlator for the noise reduction due to shielding is the average illumination angle. The EPNL reductions due to shielding were plotted against this correlator for all the cases considered in this study. A clear trend emerges of increasing EPNL reduction with decreasing average illumination angle. For average illumination angles less than 45 deg, the EPNL reduction exceeds 3 dB.

Acknowledgment

This research has been funded by Boeing Subcontract No. 208547 in support of NASA contract NNL07AA54C "Acoustic Prediction Methodology and Test Validation for an Efficient Low-Noise Hybrid Wing Body Subsonic Transport." We thank Dr. Eric Unger (Boeing) for his design of the chevron nozzles.

References

1. Von Glahn, U., Groesbeck, D., and Reshotko, M. "Geometry Considerations for Jet Noise Shielding with CTOL Engine-Over-The-Wing Concept," AIAA Paper 74-568, June 1974.
2. Von Glahn, U., Goodykoontz, J., and Wagner, J. "Nozzle geometry and forward velocity effects on noise for CTOL engine-over-the-wing concept," NASA TM-X-71453, Oct. 1973
3. Von Glahn, U., Groesbeck, and D. Wagner, J., "Wing shielding of high-velocity jet and shock-associated noise with cold and hot flow jets," AIAA Paper 76-547, July 1976.
4. Russell, J., and Berton, J., "Stone Jet Noise Module (ST2JET)", ANOPP Theoretical Manual, ver.25, NASA Langley Research Center, Hampton, VA, 2006.
5. Maekawa, Z. "Noise Reduction by Screens," *Applied Acoustics*, Vol.1, 1968, pp. 157–173.
6. Huang, C., and Papamoschou, D., "Numerical Study of Noise Shielding by Airframe Surfaces," AIAA-2008-2999, May 2008.
7. Papamoschou, D., "Pylon-Based Jet Noise Suppressors," AIAA-2008-0040, Jan. 2008.
8. Papamoschou, D., "Acoustic Simulation of Hot Coaxial Jets Using Cold Helium-Air Mixture Jets," AIAA-2005-0208, Jan. 2005.
9. "FederalAviation Regulations Part 36—Noise Standards: Aircraft Type and Airworthiness Certificiation," Federal Aviation Administration, Jan. 2002.
10. Brooks, T.F., and Humphreys, W.M., "A Deconvolution Approach for the Mapping of Acoustic Sources (DAMAS) Determined from Phased Microphone Arrays," AIAA-2004-2954, May 2004
11. Papamoschou, D., "Imaging of Distributed Directional Noise Sources," AIAA-2008-2885, May 2008.

Table 1. Cycle conditions for the BPR10 Nozzle

Quantity	Core	Fan
NPR	1.376	1.550
NTR	2.950	1.139
To (K)*	864	334
T (K)*	781	291
M	0.691	0.817
U (m/s)	387	279

*Equivalent conditions using helium-air mixture jets

Table 2 HWB shield configurations and estimated EPNL reductions.

Shield and Engine Configuration						Estimated EPNL Reductions				
X/D_f	Y/D_f	Z/D_f	Vertical	Elevator	Nozzle	ϕ=0°	30°	60°	90°	120°
No Shield					B	0	0	0	0	0
0	0	0	79°	0°	B	1.1	0.9	1	0.3	-0.1
0	0	0	Off	0°	B	0.9	0.5	0.2	-0.1	0
-1	0	0	90°	0°	B	1.2	1.6	1.3	0.5	-0.4
-1	0	0	79°	0°	B	1.2	1.1	0.8	0.2	-0.7
-2	0	0	79°	0°	B	1.6	1.6	1.3	0.1	-1.5
-1	0	0	79°	15°	B	1.9	1.6	1.2	0.1	-1.4
+1	0	0	79°	0°	B	0.3	0.4	0.2	0.3	-0.5
-1	0	0	79°	0°	W	4.9	4.3	3.8	-1.4	-3.9
0	0	0	79°	0°	W	4.1	3	1.9	0	-2.8
0	0	0	Off	0°	W	4.3	3	-0.1	-1.7	-2.8
0	0	0	79°	0°	PW	4.3	3.2	2.3	0.7	-1.1
0	0	0	79°	0°	C	3.2	2.8	3.2	2.9	0.3

X,Y,Z are fan exit locations relative to nominal engine position.
Nozzle codes: B = baseline; W = solid wedge; PW = perforated wedge; C= Chevrons

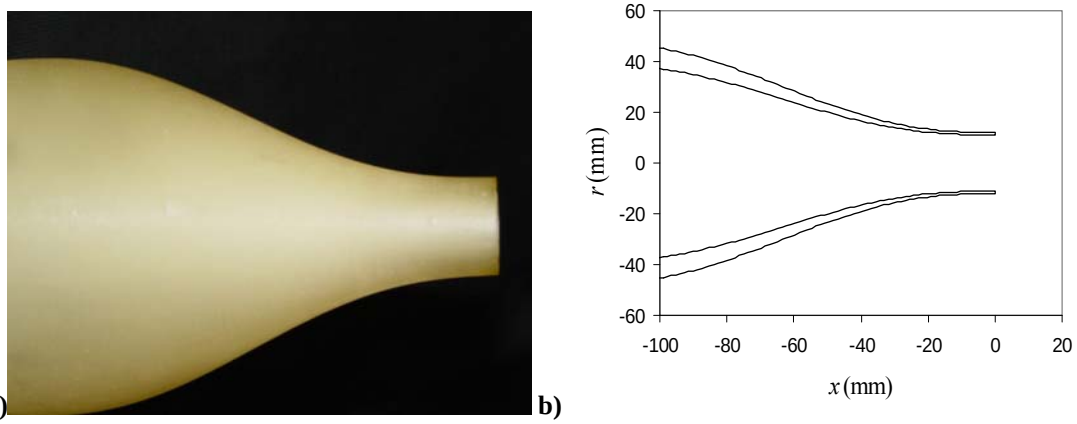

Fig. 1 Convergent single-stream nozzle used in the subscale experiments a) Picture; b) nozzle coordinates.

a)  b) 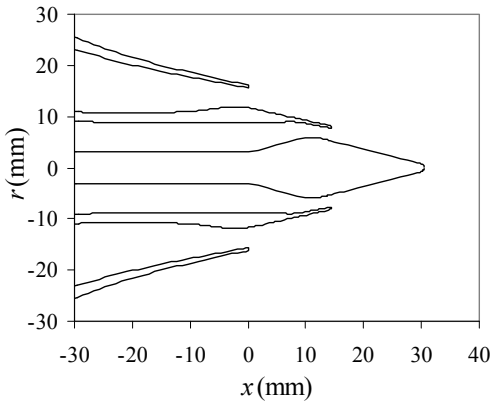

Fig. 2 BPR=10 turbofan nozzle used in the subscale experiments. a) Picture; b) nozzle coordinates.

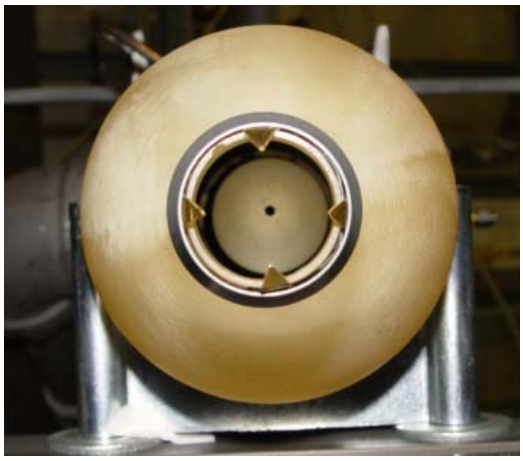

Fig. 3 Single-stream nozzle with tabs.

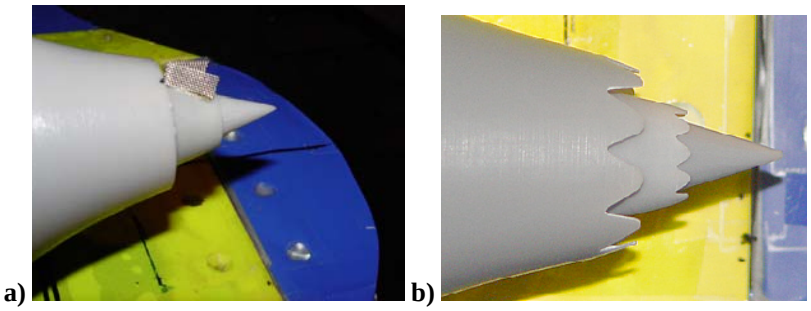

Fig. 4 BPR10 nozzle with modifications: a) perforated-flap fan flow deflector; b) Chevrons on core and fan nozzles.

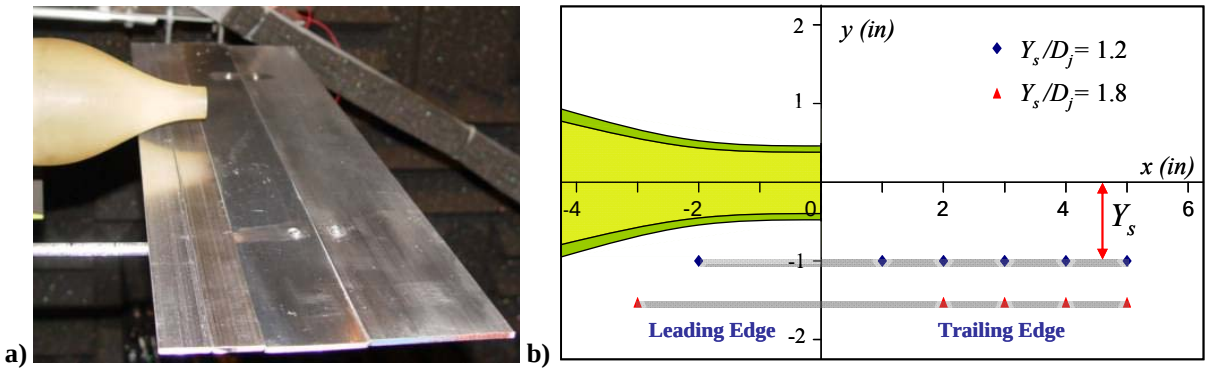

Fig. 5 a) Rectangular shielding surface using insertable strips for lengthening the chord; b) positions of leading and trailing edges of the shield.

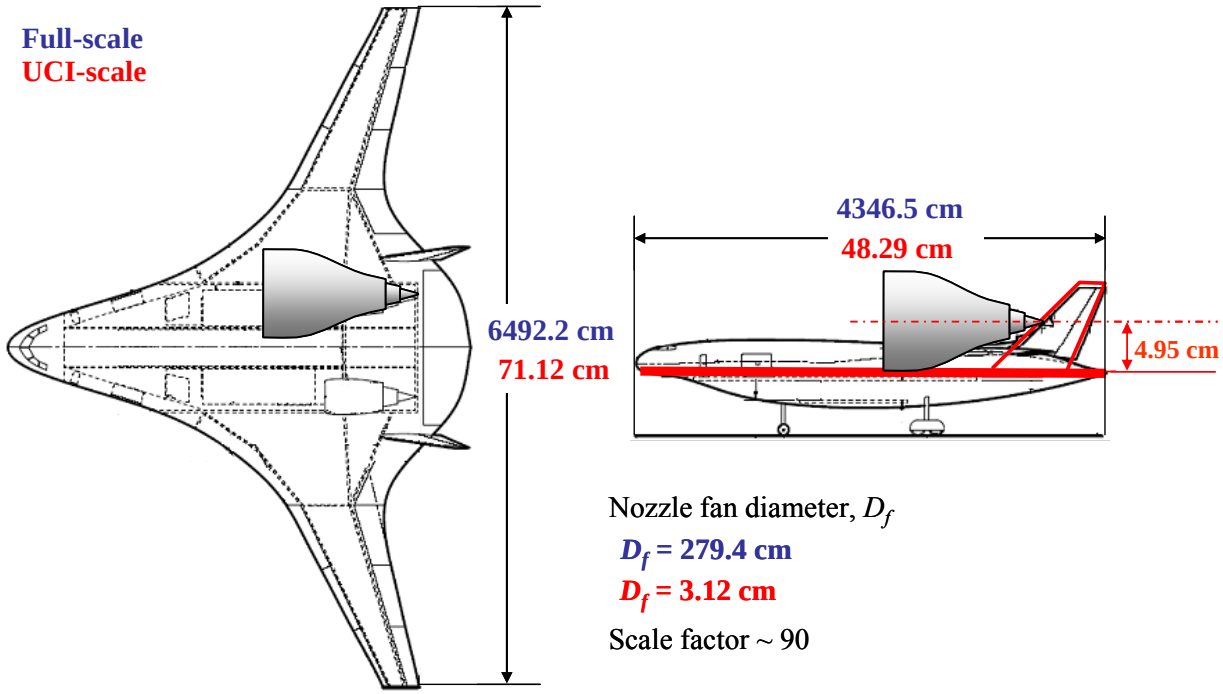

Fig. 6 Scaling of HWB planform to UCI dimensions and retention of critical dimensions for shielding (red lines).

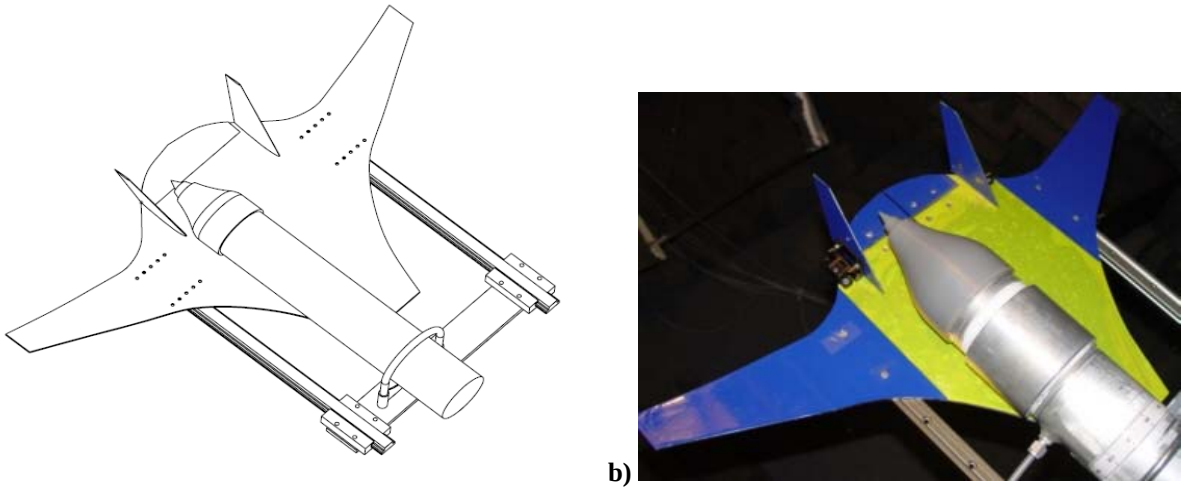

Fig. 7 a) Design of UCI HWB shield model with longitudinal traverse; b) installation with nozzle.

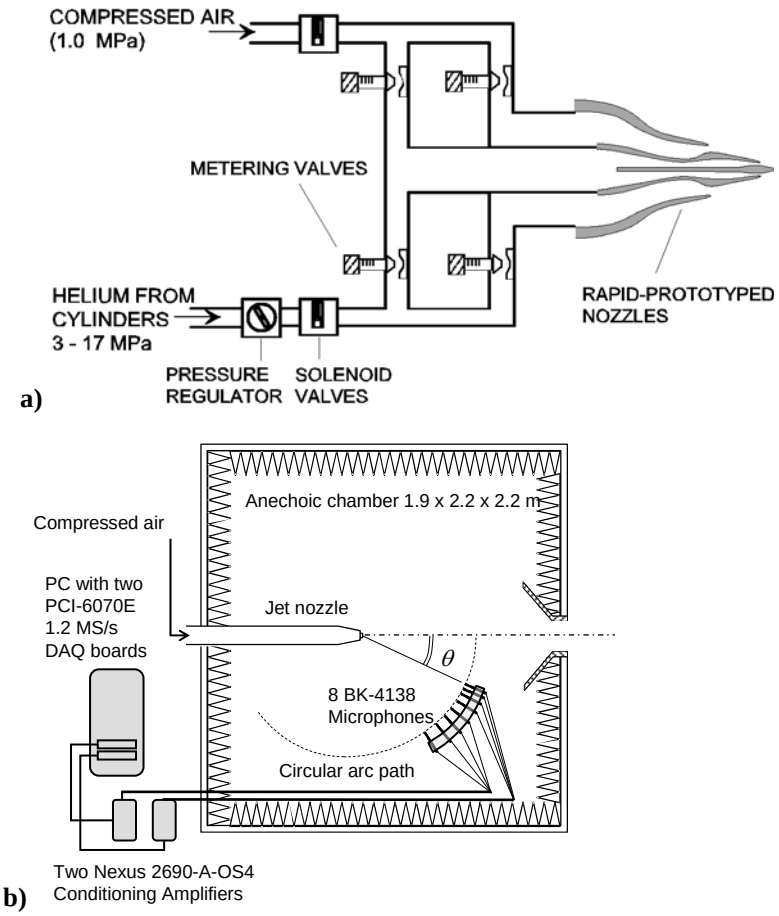

Fig. 8 UCI Jet Aeroacoustics lab. a) Flow facility; b) aeroacoustic measurement.

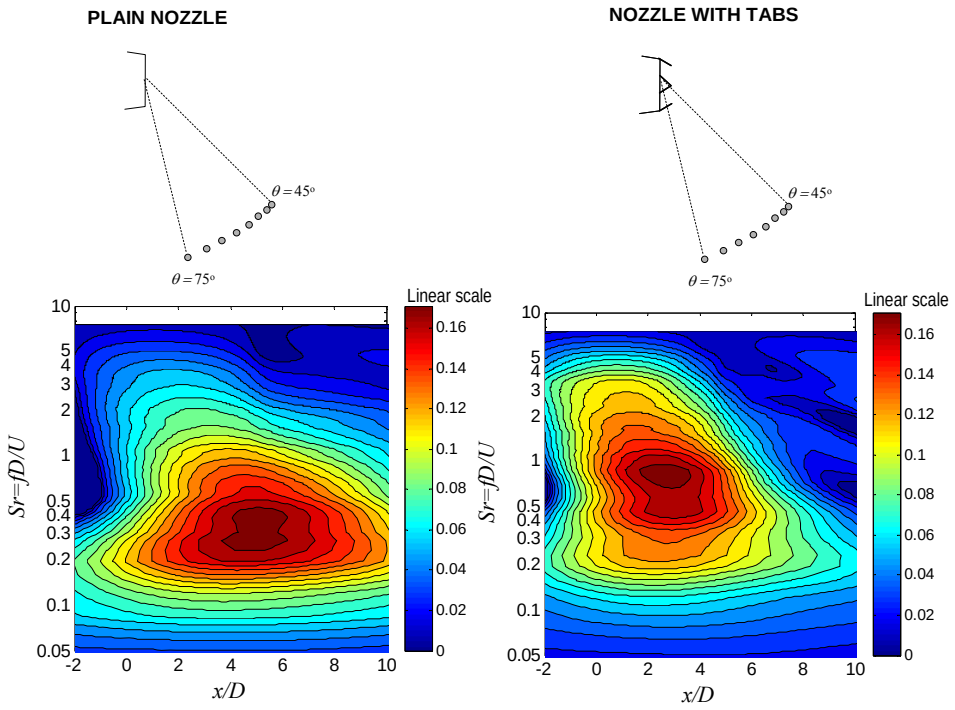

Fig. 9 Noise source maps for the single-stream nozzle and their modification by the mixing tabs.

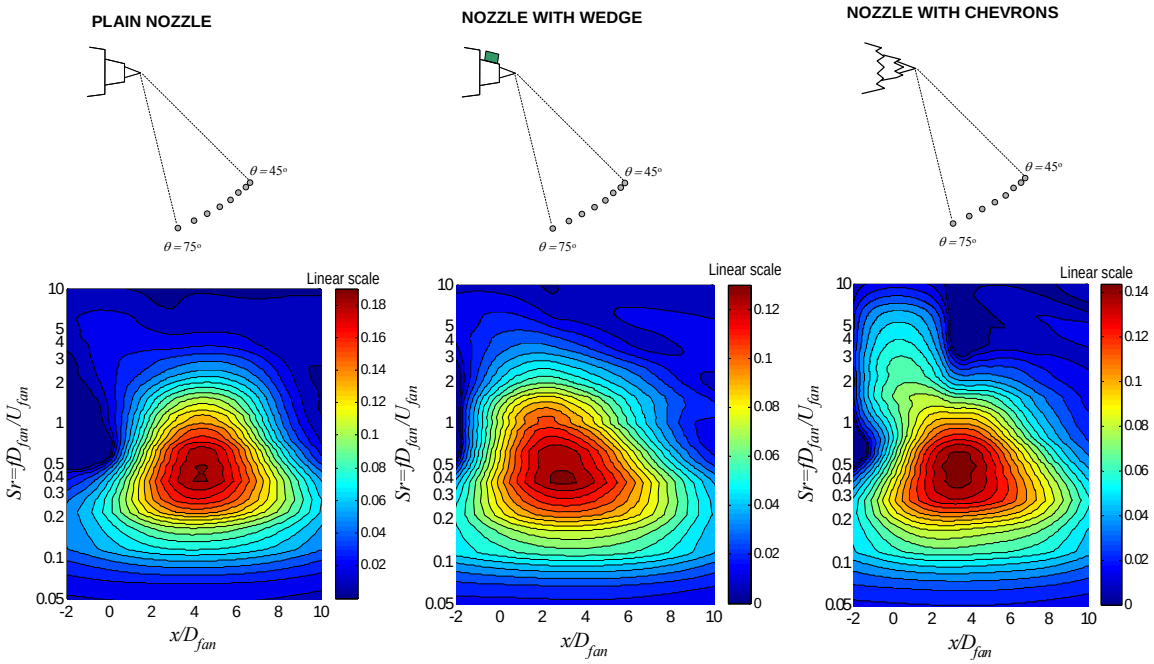

Fig. 10 Noise source maps for the BPR10 nozzle and their modification by the wedge deflector and chevrons.

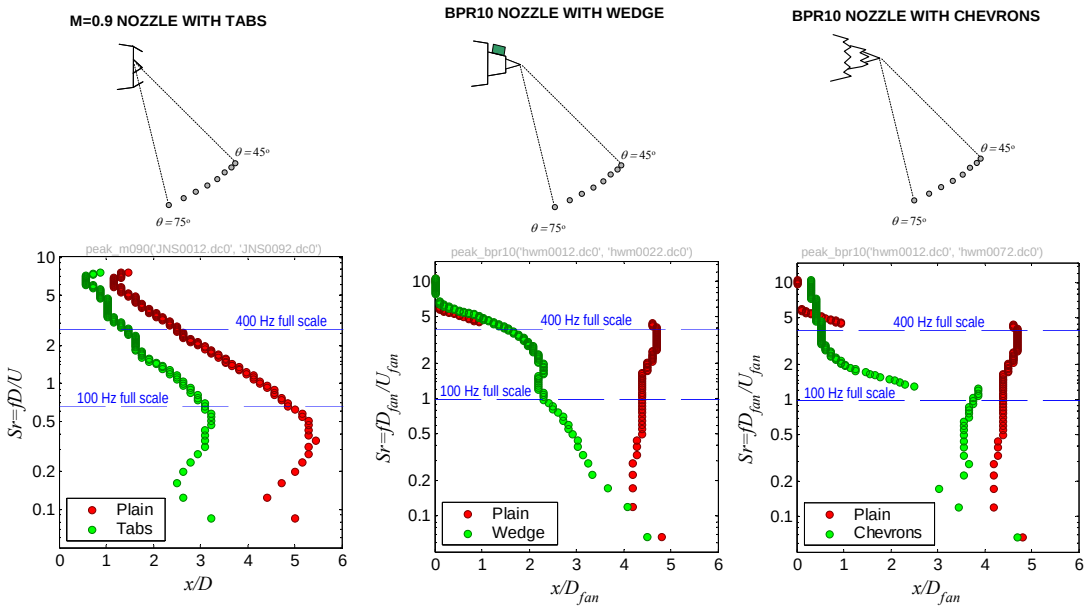

Fig. 11 Peak noise source location for single-stream the BPR10 jets without and with nozzle modifications. Dashed blue lines indicate Strouhal number band from 100 Hz to 400 Hz full-scale.

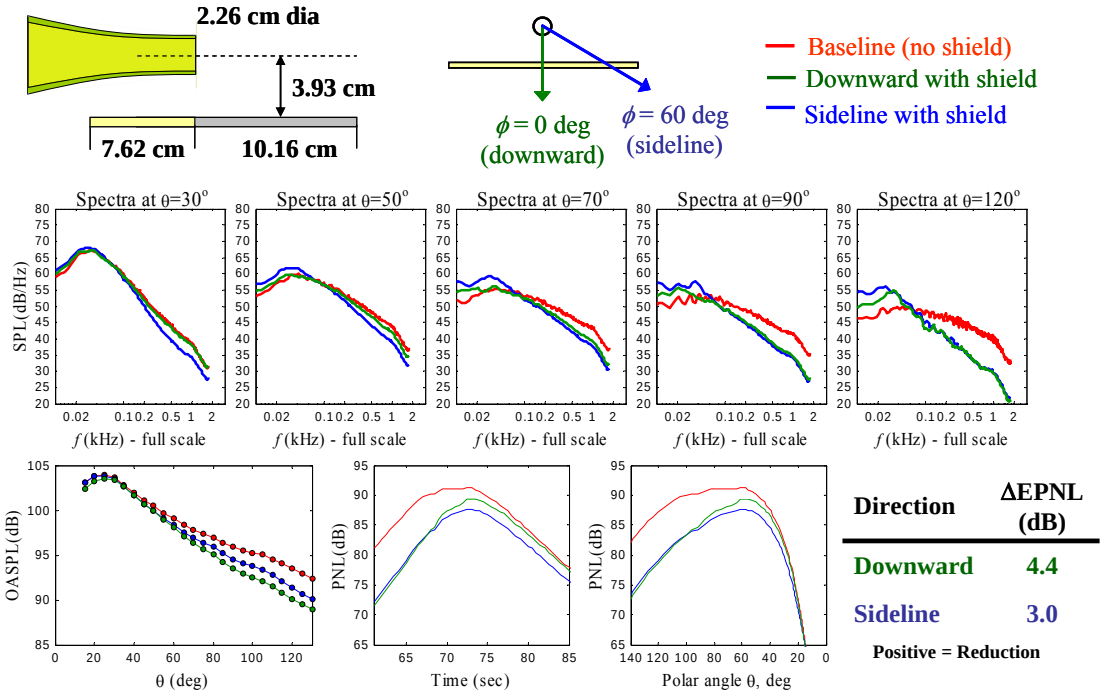

Fig. 12 Acoustic data (narrowband spectra, OASPL, PNL, EPNL) for the shielding of the M=0.90 jet issuing from plain nozzle.

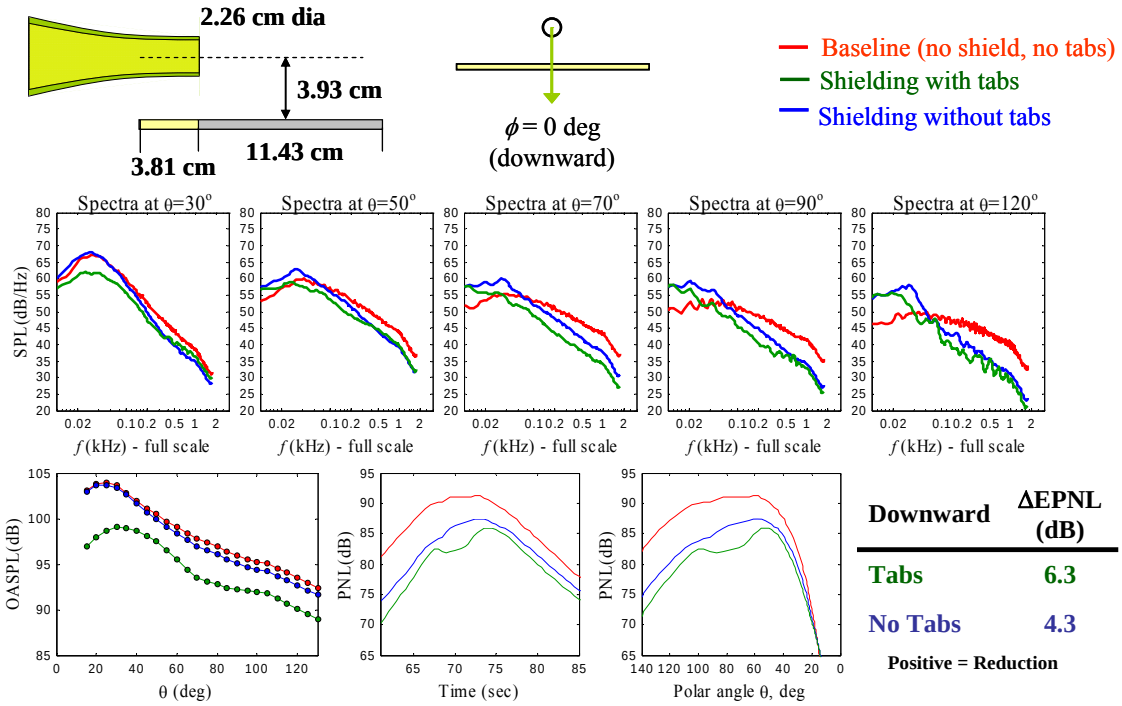

Fig. 13 Acoustic data (narrowband spectra, OASPL, PNL, EPNL) for the shielding of the M=0.90 jet issuing from plain nozzle and nozzle with tabs.

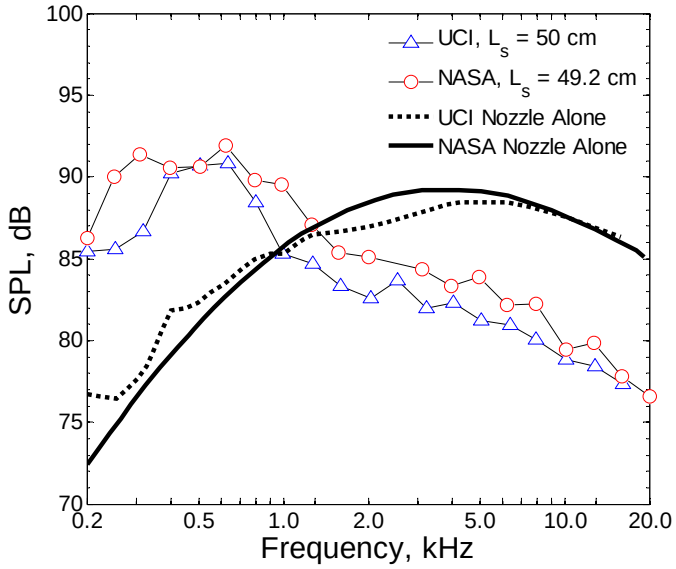

Fig. 14 UCI subscale data with the NASA full scale data for 50 cm shield length and nozzle alone case.

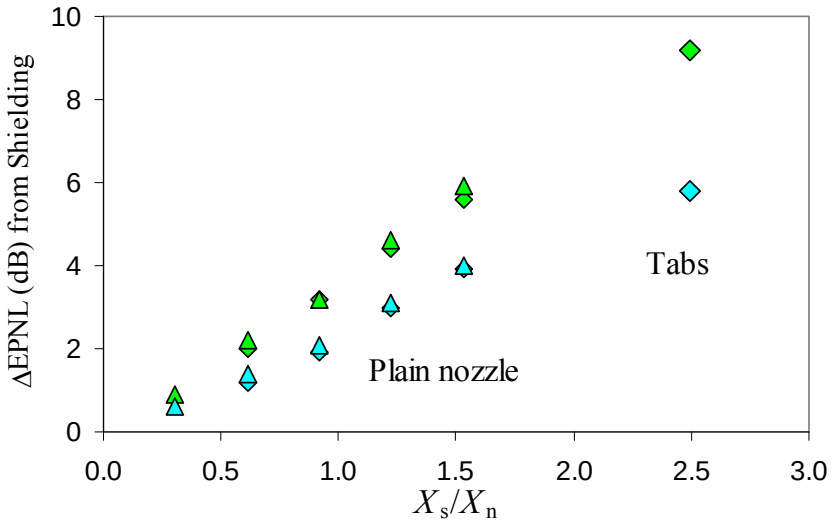

Fig. 15 EPNL reductions versus aft shield length, normalized by length of noise source region, for single-stream jet and rectangular shield. Green symbols: downward; blue symbols: sideline; diamonds: Y_s/D_j=1.8; triangles: Y_s/D_j=1.2

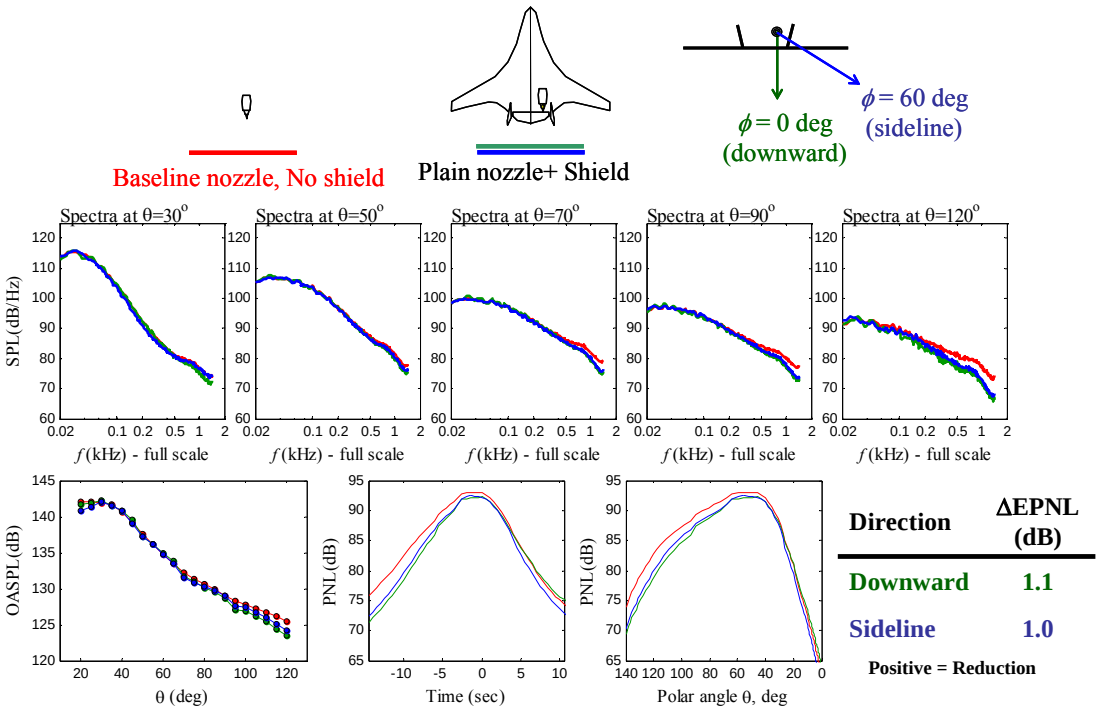

Fig. 16 Acoustic data (narrowband spectra, OASPL, PNL, EPNL) for the shielding of the BPR10 jet issuing from plain nozzle.

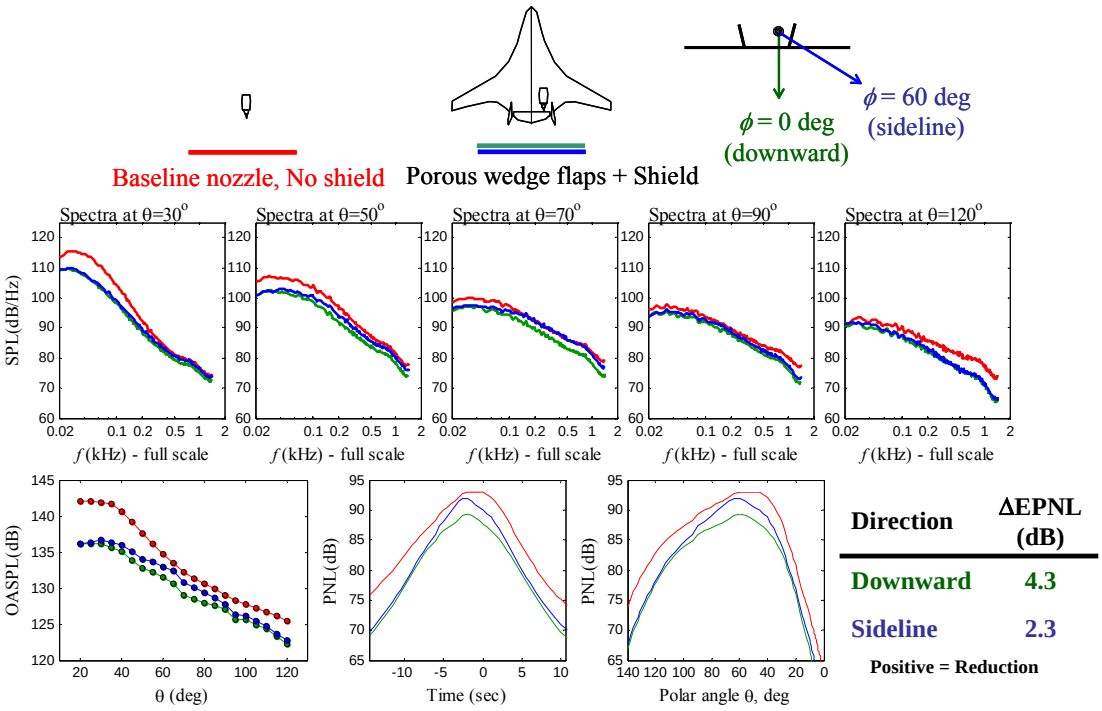

Fig. 17 Acoustic data (narrowband spectra, OASPL, PNL, EPNL) for the shielding of the BPR10 jet issuing from nozzle with perforated-flap fan flow deflector.

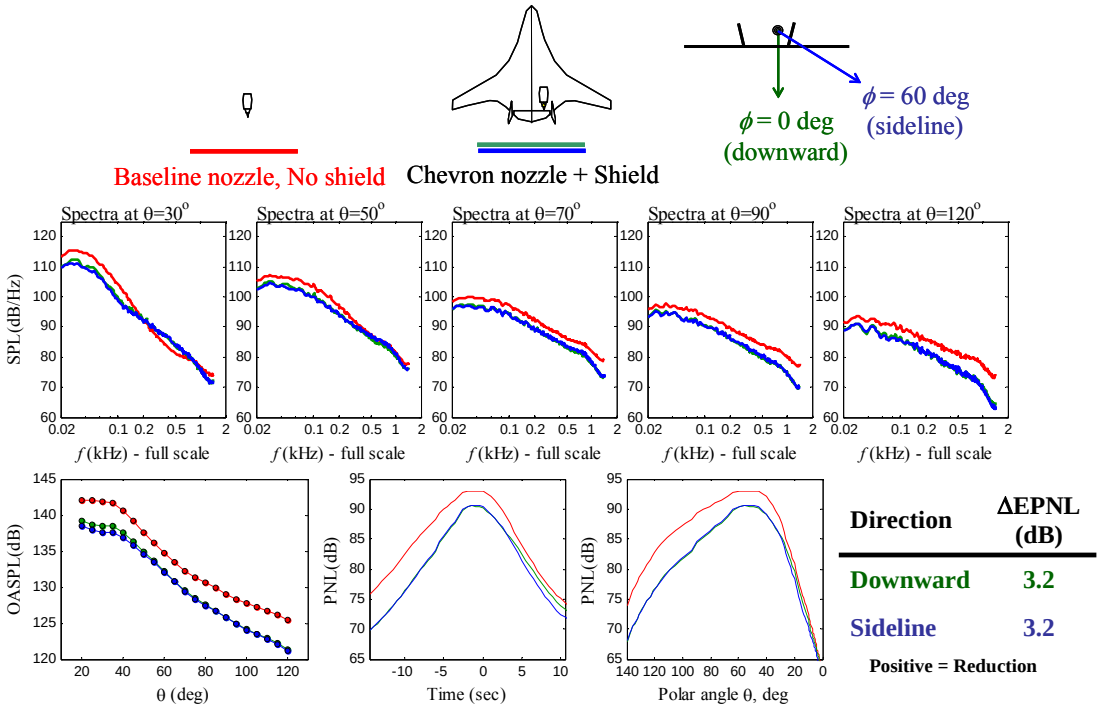

Fig. 18 Acoustic data (narrowband spectra, OASPL, PNL, EPNL) for the shielding of the BPR10 jet issuing from nozzle with aggressive chevrons (fan and core).

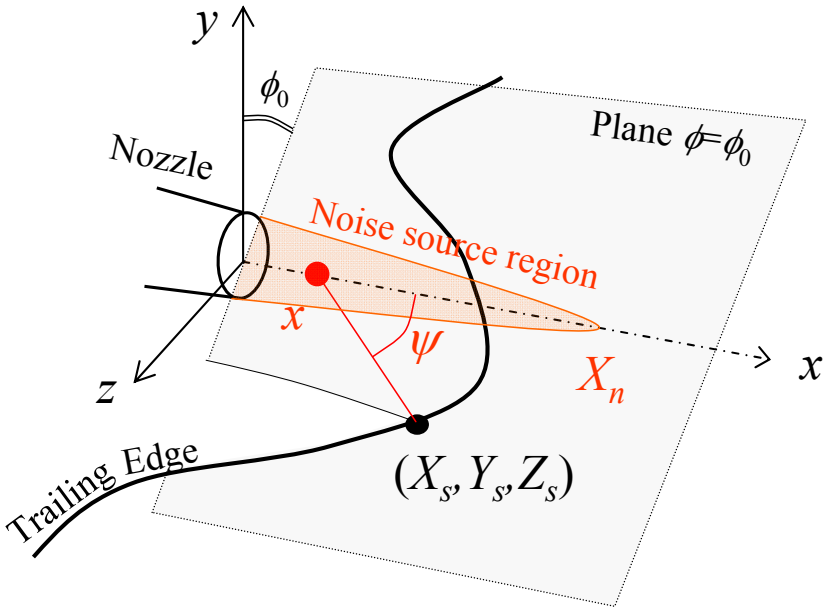

Fig. 19 Illustration of the definition of illumination angle ψ.

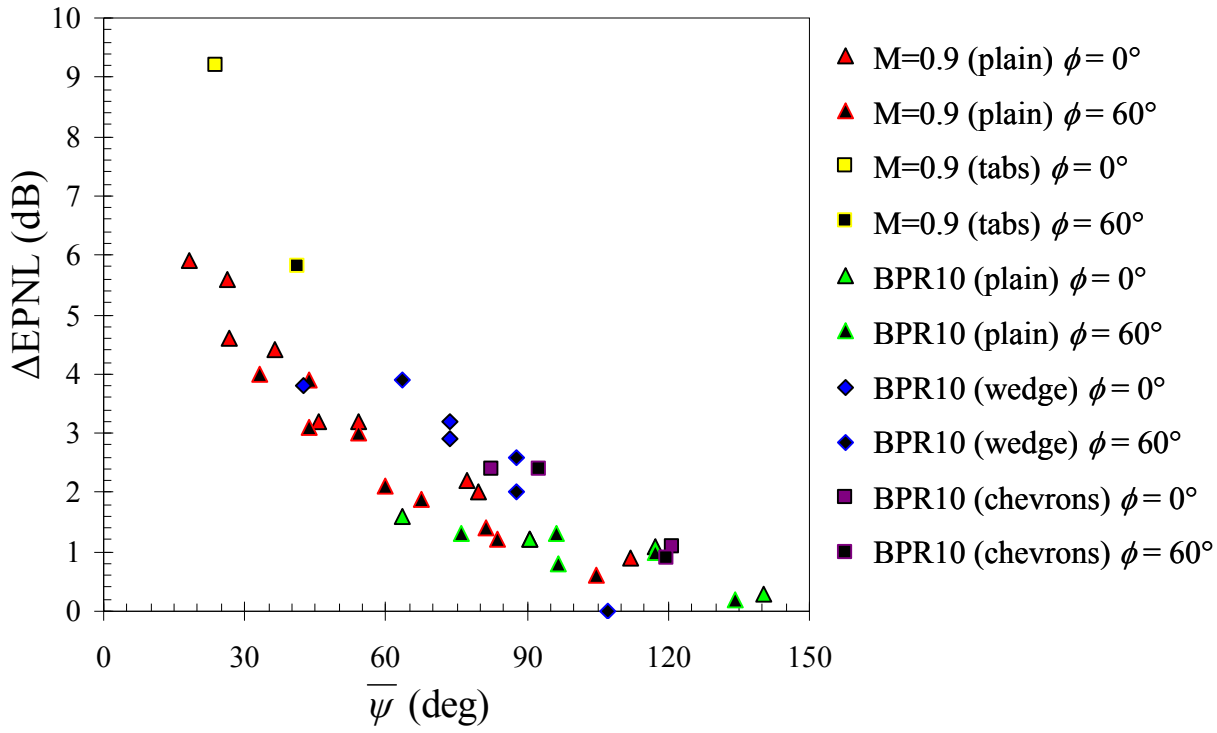

Fig. 20 Reduction of EPNL due to shielding versus average illumination angle for all the configurations studied.